Modelling of turbulent transport in arc welding pools

Nilanjan Chakraborty
CFD Laboratory, Engineering Department, Cambridge University, Cambridge, UK
Suman Chakraborty
Department of Power Plant Engineering, Jadavpur University, Calcutta, India
Pradip Dutta
Department of Mechanical Engineering, Indian Institute of Science, Bangalore, India

Received July 2001
Revised June 2002
Accepted June 2002

Keywords *Welding, Turbulence*

Abstract *In this paper, we present a modified k-ε model capable of addressing turbulent weld-pool convection in the presence of a continuously evolving phase-change interface during a gas tungsten arc welding (GTAW) process. The phase change aspects of the present problem are addressed using a modified enthalpy-porosity technique. The k-ε model is suitably modified to account for the morphology of the solid-liquid interface. The two-dimensional mathematical model is subsequently utilised to simulate a typical GTAW process with high power, where effects of turbulent transport can actually be realised. Finally, we compare the results from turbulence modelling with the corresponding results from a laminar model, keeping all processing parameters unaltered. The above comparison enables us to analyse the effects of turbulent transport during the arc welding process.*

Nomenclature

b = a small number to avoid division by zero
$\vec{B}$ = magnetic flux density
C = a large number
C_μ = proportionality constant in the formula of eddy viscosity
$C_{\varepsilon 1}$ = modelling constant for production term in ε equation
$C_{\varepsilon 2}$ = modelling constant for destruction term in ε equation
f_l = liquid fraction
f_μ = damping parameter for turbulent viscosity
g_i = Component of acceleration due to gravity in the i'th direction
ΔH = latent heat content of a control volume
h = convective heat transfer coefficient
I = welding current
$\vec{J}$ = current density
k = turbulent kinetic energy
K = thermal conductivity
L = latent heat of fusion
n = normal direction
N = Stuart Number
p = pressure
Q = arc power
q = heat flux
Re_t = turbulent Reynolds number
r_q = radius of the heat source
r_j = radius of the current source
S = source term
t = time
$\overline{T}$ = mean temperature
T' = temperature fluctuation
$\overline{U}$ = mean velocity in x-direction

International Journal of Numerical Methods for Heat & Fluid Flow
Vol. 13 No. 1, 2003
pp. 7-30

0961-5539
DOI 10.1108/09615530310456741

$\overline{U^*}$ = mean velocity in x' direction
$\overline{U}_i$ = mean velocity in i-th direction
u' = velocity fluctuation in x-direction
u_i' = velocity fluctuation in i-th direction
$\overline{V}$ = mean velocity in y-direction
v' = velocity fluctuation in y-direction
x^+ = reduced distance normal to the wall
x_i = co-ordinate direction in i-th direction
x^*, y = co-ordinate directions in stationary reference frame
x, y = co-ordinate directions in a moving reference time

Greek symbols
α = thermal diffusivity
α_t = eddy thermal diffusivity
β = coefficient of volumetric expansion
ε = dissipation rate of kinetic energy
ε_r = emissivity
ϕ = general dependent variable
μ = dynamic viscosity
μ_t = turbulent viscosity
σ = Prandtl number
σ_{elec} = electrical conductivity
σ_k = turbulent kinetic energy Prandtl number
σ_s = turbulent dissipation rate of kinetic energy Prandtl number
σ_{sur} = surface tension coefficient
σ_{rad} = Stefan-Boltzmann constant
ρ = density

Subscripts
b = black body
l = laminar
max = maximum
t = turbulent
∞ = ambient

Introduction

Welding is probably the most common process of fusion joining, in which the pieces to be joined together are locally melted by an intense energy source (such as an electric arc, laser, or plasma torch), followed by a solidification phase. The mechanical strength and microstructure of such joints are strongly dependent on the thermal histories in the fusion zone and the nearby-unmelted region during the processes. Further, fluid flow in the molten metal is known to have a considerable effect on these thermal histories and solidification processes. Therefore, in order to predict the thermal behaviour of the joint accurately, it is very much important to have a thorough knowledge of the mechanism of transport inside the weld-pool, which leads to a final resolidified microstructure. While empirical knowledge and experience have been historically employed for determining processing parameters for manual welding operations, the emerging trend of process automation has resulted in considerable scientific efforts towards optimisation of process variables for such applications.

Oreper and Szekely (1984) have first reported a detailed numerical study of weld-pool flow and thermal transport during a gas tungsten arc welding (GTAW) process. Correa and Sundell (1986) have subsequently used a modified procedure for calculation of the Lorentz force. Kanouff and Grief (1992) have used moving grids to track the phase change boundary during an arc welding process, using an evaporation model at the free surface of the weld-pool. Recognising the effects of three-dimensionality in weld-pool convection, Dutta *et al.* (1995) have developed a three-dimensional model for a GTAW process with non-axisymmetric boundary conditions. It can be noted here that all the earlier mentioned studies have typically employed laminar flow models, in order to investigate weld-pool convection mathematically. However, it can, by

no means, be precluded that the weld-pool transport would be laminar in nature. Theoretically, the nature of the transport in weld-pool (i.e. whether laminar or turbulent) can be predicted by a stability analysis, but complexities of geometry and flow impose practical restrictions towards achieving that goal. It has been observed that in case of surface tension-driven flows, the flow becomes turbulent if the surface tension Reynolds number is greater than 100 (Aboutalebi *et al.*, 1995). It can be shown that typically for the high power TIG welding, the surface tension Reynolds number is much greater than 100. Accordingly, in most welding situations where the power input is high, the weld-pool convection can be turbulent. Experimentally it has been observed by Joshi *et al.* (1997) that under high current conditions, there can be perceptible surface oscillations in the pool. Moreover, the resultant pool is shallower in practice than that predicted by familiar laminar fluid flow models. Such oscillations could be due to surface instabilities, which might eventually lead to turbulence. The above is also in accordance with an earlier work reported by Atthey (1980), where the author mentioned the possibility of onset of turbulence in weld-pools under conditions of high arc current. Hence, it is important to investigate the effects of turbulence during fusion welding processes.

Turbulence modelling in the context of materials processing, in general, is a relatively recent practice (Aboutalebi *et al.*, 1995; Shyy *et al.*, 1992). Most of the researchers in this field have preferred k-ε model for its well-known advantages over other available models. In order to account for turbulent transport phenomenon in welding applications, Mundra *et al.* (1992) have examined the effect of varying the fluid viscosity in their mathematical model of laser welding. However, enhancement of thermal diffusivity due to turbulence was not taken into account in their model.

Additionally, the variation of viscosity in the earlier investigation was treated rather intuitively. More recently, Chao and Szekely (1994) have modelled the effects of turbulence in stationary GTAW weld-pools using k-ε models. However, the treatment of solid-liquid interface with regard to the implementation of wall conditions was not elaborately addressed in their work. Recently, Hong *et al.* (1995) have developed a finite element based model to study the effect of turbulence by taking variable surface tension coefficient, which can vary with temperature and composition of surface active elements. It can be noted here that in none of the earlier investigations, the mathematical details of k-ε modelling, as modified for welding applications, have been adequately discussed. Also, effects of phase change and dynamic evolution of the resultant solid-liquid interfaces have not been incorporated in the models. From the earlier mentioned studies, it is clear that there is a need to develop a detailed formulation for turbulence modelling in the context of arc weld-pool convection.

The aim of the present work is to develop a modified k-ε model capable of addressing turbulent weld-pool convection in the presence of a continuously evolving phase-change interface during a GTAW process. In order to take into account the phase change aspects of the present problem, a modified enthalpy-porosity technique is used. The source terms of both k and ε equations are so devised that a smooth transition from a completely solid state to a fully liquid state can be achieved by the same set of equations. Dynamic conditions at the interface are inherently tackled by resorting to a moving coordinate system and prescribing appropriate wall conditions at solid-boundary locations that evolve continuously with time. It may be noted here that the present study is only aimed towards the development of a turbulence model for application in weld-pool convection. For the sake of simplicity in implementation, we have used a two-dimensional model and discussed some issues pertaining to turbulent weld-pool convection in a qualitative sense only. It is expected that most of the trends observed in the two-dimensional model would still be valid in realistic three-dimensional situations. The two-dimensional mathematical model is subsequently utilised to simulate a typical GTAW process with high power, where effects of turbulent transport can actually be realised. Finally, we compare the results from turbulence modelling with the corresponding results from a laminar model, keeping all processing parameters unaltered. The earlier comparison enables us to analyse the effects of turbulent transport during the welding process.

Mathematical formulation

Governing equations for heat and fluid flow

In the GTAW welding process, the arc is maintained between a non-consumable tungsten electrode and the work-piece in a protective inert gas atmosphere. Figure 1 shows a schematic diagram of the process. As shown in

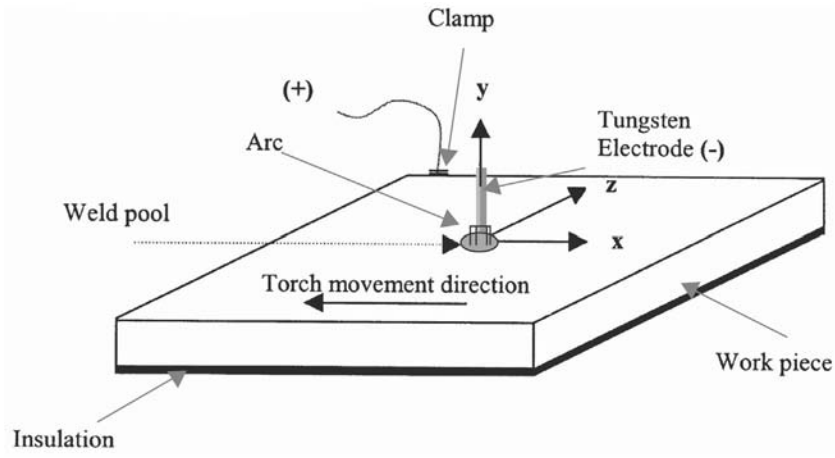

Figure 1.
A schematic diagram of the model problem

Figure 1, the electrode is moving with a constant speed (U_{scan}) in the negative x direction. The arc heat is responsible for heating the work-piece. Only a part of energy of arc heat actually heats the surface of the work-piece, and that heat is transported by diffusion and convection mechanism to other parts of the work-piece that eventually leads to the formation of a molten pool. We assume the input energy to the work-piece is in the form of a Gaussian heat source. A considerable amount of energy is lost from the work-piece to the surroundings due to convective and radiative heat transfer. The actual power that goes to the work-piece is specified by arc efficiency, η. The following relation relates the available heat to power input:

$$q = \eta Q = \eta VI \tag{1}$$

where V and I are specified arc voltage and arc current, respectively. As the work-piece melts, the absorbed energy induces a predominantly surface tension-driven flow at the top surface, which redistributes the fluid momentum as well as the thermal energy, turbulent kinetic energy, and dissipation of turbulent kinetic energy inside the molten pool. The electromagnetic (Lorentz) force and buoyancy forces also comes into play, but in most cases their strengths are about an order of magnitude lower than surface tension (Marangoni) forces (Chakraborty *et al.*, 2001). It can be noted that in case of turbulent flow, both convection and diffusion mechanisms may be of importance and relative strength of these two mechanisms ultimately determines the shape and size of the molten pool.

The following assumptions are made in modelling the present problem.

(1) The dependence of surface tension with temperature is assumed to be linear.

(2) The top surface of the melt pool is assumed to be flat.

(3) The eddy viscosity is calculated using a two-equation k-ε turbulence model.

(4) The flow of molten metal is Newtonian and incompressible.

(5) For simplicity, the welding process is assumed to be two-dimensional, with the Gaussian arc heat input having a unit depth perpendicular to the plane of the paper. It may be noted here that the aim of the present work is to establish a turbulent weld-pool model and highlight the fundamental difference between a laminar and turbulent weld-pool behaviour. Since, in this study, we are not specifically looking for numerical accuracy of prediction by comparing with experimental moving arc weld-pools (which are inherently three-dimensional in nature), a two-dimensional model can be more conveniently used to satisfy our primary objective.

The generalised governing transport equation in the weld-pool and its surroundings in a stationary coordinate system (x^*,y) can be written as:

$$\frac{\partial(\rho\phi)}{\partial t}+\frac{\partial(\rho\overline{U^*}\phi)}{\partial x^*}+\frac{\partial(\rho\overline{V}\phi)}{\partial y}=\frac{\partial}{\partial x^*}\left(\Gamma\frac{\partial\phi}{\partial x^*}\right)+\frac{\partial}{\partial y}\left(\Gamma\frac{\partial\phi}{\partial y}\right)+S \qquad (2)$$

where ϕ is any dependent scalar variable, Γ is a generalised diffusion coefficient, and S is a source term. However, the transport phenomenon occurring inside the weld-pool can be conveniently studied with respect to a coordinate system that translates with the arc heat source. Accordingly, we introduce the following coordinate transformation:

$$x = x^* - U_{\text{scan}}t \qquad (3)$$

where U_{scan}, is the speed of welding torch and x,y are coordinates in a frame moving with the torch. Henceforth, we will follow the following tensorial notation for description of conservation equation:

$$\begin{aligned} x_1 &= x \\ x_2 &= y \end{aligned} \qquad (4)$$

Carrying out the transformation described in equation (3) and noting that the scanning is done in negative x^* direction, we obtain:

$$\frac{\partial(\rho\phi)}{\partial t}+\frac{\partial(\rho\overline{U}_j\phi)}{\partial x_j}=\frac{\partial}{\partial x_j}\left(\Gamma\frac{\partial\phi}{\partial x_j}\right)+S-\frac{\partial(\rho U_{\text{scan}}\phi)}{\partial x_1} \qquad (4a)$$

Substituting ϕ by appropriate transport variables, the governing equations in the moving coordinate system assume the following forms:

Conservation of mass (continuity equation). The single-phase continuity equation for an incompressible fluid is given by:

$$\frac{\partial\overline{U}_i}{\partial x_i}=0; \quad \frac{\partial u_i'}{\partial x_i}=0 \qquad (5)$$

where the superscript ('/') represents the fluctuating component of a scalar variable.

Conservation of linear momentum. The equivalent single-phase linear momentum conservation equation for the ith direction is given by $i = 1, 2$:

$$\frac{\partial(\rho\overline{U}_i)}{\partial t}+\rho\overline{U}_j\frac{\partial\overline{U}_i}{\partial x_j}=-\frac{\partial p}{\partial x_i}+(\vec{J}\times\vec{B})_i+\frac{\partial}{\partial x_j}\left(\mu\frac{\partial\overline{U}_i}{\partial x_j}\right)-\frac{\partial\left(\rho\overline{u_i'u_j'}\right)}{\partial x_j}$$

$$-\rho U_{\text{scan}}\frac{\partial\overline{U}_i}{\partial x_1}+\rho g_i\beta(\overline{T}-T_{\text{ref}})+\overline{S}_i \qquad (6)$$

where g_i is the component of acceleration due to gravity in the ith direction, and T_{ref} is taken to be equal to the melting temperature, T_m. The source term $\overline{S}_i$ in equation (6) originates from the consideration that the morphology of the phase change domain can be treated as an equivalent porous medium that offers a frictional resistance towards fluid flow in that region. In a single-domain fixed-grid enthalpy-porosity formulation, this resistance can be conveniently formulated using Darcy's model in conjunction with the Cozeny-Karman relationship (Brent *et al.*, 1988). In equation (6), $\overline{S}_i$ is given as:

$$\overline{S}_i = -\frac{C(1-f_1^2)}{f_1^3+b}\overline{U}_i \tag{6a}$$

where $f_1 = \Delta H/L$, with ΔH being the latent enthalpy content of a control volume and L being the latent heat of fusion. In equation (6a), C is a large number ($\sim 10^8$) and b is a small number ($\sim 10^{-30}$) to avoid division by zero. The earlier formulation effectively ensures that the velocity undergoes a smooth transition from a zero value in solid region to a finite value in the fully liquid region. The details of formulation of the earlier term can be found in Brent *et al.* (1988). The term $-\partial/\partial x_j(\rho\overline{u_i'u_j'})$ is called Reynolds stress term, the modelling of which is detailed subsequently. The Lorentz force term $\vec{J}\times\vec{B}$ is evaluated by solving Maxwell's equations. The mathematical formulation and numerical procedure for the solution of Maxwell's equations are detailed by Dutta *et al.* (1995).

Conservation of energy. The single-phase energy equation for turbulent flow is given by:

$$\frac{\partial(\rho\overline{T})}{\partial t}+\frac{\partial(\rho\overline{U}_i\overline{T})}{\partial x_i}=\frac{\partial}{\partial x_i}\left(\frac{K}{c}\frac{\partial\overline{T}}{\partial x_i}\right)-\frac{1}{c}\frac{\partial(\rho\Delta H)}{\partial t}-\frac{\partial}{\partial x_i}\left(\frac{\rho}{c}\overline{U}_i\Delta H\right)$$
$$-\frac{1}{c}\frac{\partial(\rho\overline{u_i'T'})}{\partial x_i}-\rho U_{scan}\frac{\partial\overline{T}}{\partial x_i} \tag{7}$$

where c is the specific heat of the material, K is the thermal conductivity, and ΔH is the latent enthalpy content of the computational cell under consideration. In the present study, we assume the material to behave as a pure metal, and hence the phase change is isothermal. For such a case,

$$\Delta H=\begin{cases} L & \overline{T}>T_m \\ 0 & \overline{T}\le T_m \end{cases} \tag{8}$$

Modelling of Reynolds stress terms ($-\rho\overline{u_i'u_j'}$)

In the present analysis, we model the Reynolds stress terms appearing in equation (6) by assuming a turbulent viscosity of the form:

$$-\rho\overline{u_i'u_j'} = \mu_t\left(\frac{\partial\overline{U}_i}{\partial x_j} + \frac{\partial\overline{U}_j}{\partial x_i}\right) - \frac{2}{3}\delta_{ij}k \tag{9}$$

where

$$\mu_t = f_\mu C_\mu \rho k^2/\varepsilon \tag{9a}$$

In equation (9a), C_μ is a constant, whose value has been experimentally determined from shear flow experiments. It is reported that C_μ varies from 0.08 to 0.09 (Komatsu and Matsunaga, 1986). The term f_μ in equation (9a) is a damping function, which damps the effect of, μ_t as the solid wall is approached. In reality, f_μ, is a very important parameter because it acts as a parameter of proportionality in the computation of, μ_t in k-ε model. In a standard k-ε model, f_μ is taken as a constant, equal to 1.0. However, in the present problem, the whole domain is not composed of a single phase. Accordingly, the formulation should ensure an asymptotic reduction of eddy viscosity and thermal conductivity to their respective molecular values along the solid-liquid interface, and merge with single-phase turbulent flow conditions in the fully liquid region. To satisfy the earlier requirement, the following correlation between f_μ and f_1 can be used (Shyy *et al.*, 1992).

$$f_\mu = \exp\left(\frac{-3.4}{\left[1+\frac{\mathrm{Re}_t}{50}\right]^2}\right)\sqrt{f_1} \tag{10}$$

where

$$\mathrm{Re}_t = \frac{\rho k^2}{\varepsilon\mu} = \text{Turbulent Reynolds number} \tag{10a}$$

Modelling of turbulent heat fluxes ($-\rho\overline{u_i'H'}$)

Following the same analogy as the Reynolds stresses, the turbulent heat fluxes (Reynolds heat fluxes) appearing in equation (7) can be written as:

$$-\frac{\overline{u_j'H'}}{c} = -\overline{u_j'T'} = \alpha_t\frac{\partial\overline{T}}{\partial x_j} \tag{11}$$

where α_t is the eddy thermal diffusivity. From the analogy of laminar flow, α_t can be expressed as:

$$\alpha_t = \frac{\mu_t}{\rho \sigma_t} \tag{11a}$$

where σ_t is turbulent Prandtl number. It has been proposed that σ_t varies from 0.8 to 0.9.

In the present work, we take $\sigma_t = 0.9$

Governing equations for k and ε. The governing equations for k and ε in the present context can be written as:

$$\frac{\partial(\rho k)}{\partial t} + \overline{U}_j \frac{\partial k}{\partial x_j} = \frac{\partial}{\partial x_j}\left[\left(\mu + \frac{\mu_t}{\sigma_k}\right)\frac{\partial k}{\partial x_j}\right] + \mu_t\left(\frac{\partial \overline{U}_i}{\partial x_j} + \frac{\partial \overline{U}_j}{\partial x_i}\right)\frac{\partial \overline{U}_i}{\partial x_j} - \frac{\mu_t}{\sigma_t} g\beta \frac{\partial \overline{T}}{\partial x_2} - \rho\varepsilon - \rho U_{scan}\frac{\partial k}{\partial x_1} \tag{12}$$

$$\frac{\partial(\rho\varepsilon)}{\partial t} + \overline{U}_j \frac{\partial(\rho\varepsilon)}{\partial x_j} = \frac{\partial}{\partial x_j}\left[\left(\mu + \frac{\mu_t}{\sigma_e}\right)\frac{\partial \varepsilon}{\partial x_j}\right] + C_{\varepsilon 1}\mu_t\left(\frac{\partial \overline{U}_i}{\partial x_j} + \frac{\partial \overline{U}_j}{\partial x_i}\right)\frac{\partial \overline{U}_i}{\partial x_j}\frac{\varepsilon}{k} - C_{\varepsilon 1}\frac{\mu_t}{\sigma_t} g\beta \frac{\partial \overline{T}}{\partial x_2}\frac{\varepsilon}{k} - C_{\varepsilon 2}\frac{\rho\varepsilon^2}{k} - \rho U_{scan}\frac{\partial \varepsilon}{\partial x_1} \tag{13}$$

where

$$C_\mu = 0.09, \quad C_{\varepsilon 1} = 1.44, \quad \text{and} \quad C_{\varepsilon 2} = 1.92$$
$$\sigma_k = 1.0, \quad \sigma_\varepsilon = 1.3$$

Boundary conditions

The boundary conditions for the flow variables with reference to the work piece can be stated as follows:

Top surface. Considering Gaussian heat input, convective and radiation loss, we write the following boundary condition:

$$-K\frac{\partial \overline{T}}{\partial y} = -q''(r) + h(\overline{T} - T_\infty) + \varepsilon_r \sigma_{rad}(\overline{T}^4 - T_\infty^4) \tag{14}$$

where $q''(r)$ is the net arc heat flux distributed in a Gaussian manner with a radius of r_q,ε_r is the Emissivity of the top surface and σ_{rad} is the Stefan-Boltzmann constant. From the flat surface condition at the top, we get:

$$\overline{V} = 0 \tag{15}$$

From the free surface shear balance between viscous force and surface tension:

$$\mu \frac{\partial \overline{U}}{\partial y} = \frac{\partial \sigma_{sur}}{\partial T} \frac{\partial \overline{T}}{\partial x} \tag{16}$$

where σ_{sur} is the surface tension.

Regarding the transport of k and ε, we assume that the top surface acts like a rigid lid (Aboutalebi *et al.*, 1995) and write:

$$\frac{\partial k}{\partial y} = 0 \tag{17}$$

$$\frac{\partial \varepsilon}{\partial y} = 0 \tag{18}$$

Side faces. The four side faces are subjected to convective heat transfer boundary condition:

$$-K\left(\frac{\partial T}{\partial n}\right)_{\text{wall}} = h(T - T_{\infty}) \tag{19}$$

where n is the direction of outward normal to the surface concerned.

Bottom face. The face being insulated, the temperature boundary condition is:

$$\left(\frac{\partial T}{\partial y}\right)_{\text{bottom}} = 0 \tag{20}$$

Solid/liquid interface. It is apparent that the solid/liquid interface in this problem acts as a wall, and the same needs to be treated appropriately. However, according to the enthalpy-porosity formulation, we need not track the interface separately and impose velocity or temperature boundary conditions on the same, since the interface comes out as a natural outcome of the solution procedure itself. However, the evolving interface locations are important inputs for k and ε equations, since the values of k and ε are to be specified for near wall points with the help of suitable wall functions, which leads to satisfaction of the following conditions at the solid/liquid interface:

$$k = 0 \tag{21}$$

$$\frac{\partial \varepsilon}{\partial n} = 0 \tag{22}$$

Numerical procedure

With an assumption that the electric current flowing through the work-piece is steady and there is no coupling between fluid flow and electric current, the governing equations for electromagnetic force field are solved numerically, *a priori*, to calculate the Lorentz force field. The solution procedure for obtaining the Lorentz force field (i.e. $\vec{J} \times \vec{B}$) is outlined in detail by Dutta *et al.* (1995), and is not repeated here for the sake of brevity. The calculated Lorentz force field is subsequently used as body force distribution in the momentum equations. The coupled continuity, momentum, energy, k and ε equations are solved simultaneously using a pressure-based semi-implicit finite volume technique according to the SIMPLER algorithm (Patankar, 1980). We have used the power law scheme (Patankar, 1980) for differencing the convective terms. In the numerical solution of the energy equation, the latent heat content of each control volume is updated using the temperature field predicted from the energy equation, as outlined by Brent *et al.* (1988). In a physical sense, the updating of the latent heat term attempts to neutralise the difference in temperature as obtained from the energy equation and that dictated by phase change consideration, in order to obtain a physically realistic converged solution.

The turbulence aspects of the present numerical code are first validated against a previous work done by Chang (1984) for recirculating turbulent flow in a two-dimensional symmetric step channel. The results (not shown here) are compared with results from the earlier study, and they match well. The phase change aspects of the present code are tested against numerical results reported by Brent *et al.* (1988), corresponding to the melting of pure Gallium in a rectangular cavity, and an excellent agreement is obtained.

Results and discussion

Numerical simulations are performed for the case of a GTAW situation with steel as the base material. The thermophysical properties and processing parameters for the problem are listed in Table I. The size of the computational domain is taken as 45×15 mm for the solution of heat and fluid flow equations.

Choice of grid-size

In order to capture the top surface velocity originating from surface tension gradients, the choice of grid-size should be judicious. This also ensures indirectly that the calculations for velocity gradients are accurate enough, so that the turbulent source terms can be properly evaluated. Accordingly, we adopt the following criteria for the choice of grid-size for the present simulation.

Criterion-1. At the top surface of the pool, surface tension forces are caused by steep temperature gradients as per equation (16). In order to obtain an estimate of the viscous boundary layer thickness (δ_v) at the top that is caused by the resultant surface tension driven flow, an appropriate scaling analysis is

Physical property	Value
Volumetric expansion coefficient (β)	0.00001 K^{-1}
Melting temperature (T_m)	1,500°C
Latent heat of fusion (L)	247,196 J/kg
Density (ρ)	7,800 kg/m^3
Thermal conductivity (K)	35 W/mK
Specific heat (c)	753 J/kg
Molecular viscosity (μ)	0.006 Pa s
Surface tension coefficient (σ)	0.0005 N/m K
Problem data	*Value*
Arc voltage (V)	12 V
Arc current (I)	150 Amp
Arc efficiency (η)	90%
Scanning speed (u_{scan})	7.62 mm/s

Table I.
Table of physical properties and problem data

performed with respect to the stationary molten pool for the laminar case. Following a procedure outlined by Dutta *et al.* (1995), and using the typical thermophysical parameters for the model problem solved in this study, we obtain the velocity boundary layer thickness of the order of 10^{-5} m. Accordingly, in order to capture sufficient flow details inside the surface tension driven boundary layer, at least a few (typically five) grid points are accommodated inside it.

Criterion-2. In order to specify the diffusion coefficients near the wall, it is necessary to control the grid-size in its vicinity. Otherwise it may so happen that the grid points immediately next to the wall may fall beyond the "near wall" regime. However, if the diffusion coefficients are still evaluated by log-law, the simulation may lead to an underestimation of diffusion coefficient and one can end up with unrealistic results eventually. Hence, it is necessary to have a grid distribution such that the grid next to the wall always falls within the buffer layer. This condition is mathematically given by:

$$x^+ \leq 30 \tag{23}$$

where

$$x^+ = \frac{\rho k^{0.5} x}{\mu} \tag{23a}$$

One can satisfy the earlier requirement by ensuring that x^+ remains within 30, even for the maximum possible value of k. However, it unnecessary calls for very fine grid that can increase the computational costs considerably, since, in practice, the value of k is typically low near the walls. The appropriate grid-size, which can meet the earlier requirement, is best found by trial and error method using limiting values of k.

From the two requirements discussed earlier it is evident that the grid spacing in y direction is governed by criterion 1, and that in the x-direction is determined by criterion 2. Accordingly, we choose a depth of 2.7×10^{-7} m for the topmost grids. Just below this, the grid depth is taken as 1.35×10^{-6} m, followed by a depth of 3.5×10^{-5} m. Thereafter a uniform grid depth of 1×10^{-4} m is employed for most of the remaining part of the pool. The grid spacing is made coarser in y-direction gradually. Outside the molten pool, a non-uniform coarser grid is chosen. In the x-direction, an optimised grid size near the wall is found to be 5×10^{-4} m, after which the grid-size is increased gradually as we move away from the wall. It is found that a finer grid system is not found to alter the results appreciably. Overall, a (40×36) grid system is used to discretise the working domain $(45 \times 15\,\text{cm})$.

Choice of time step

For the model system studied in the present investigation, initiation of melting takes about 0.25 s. Before melting, there is a conduction-dominated regime, during which a large time step (of about 0.05 s) is chosen for computational economy. However, once melting starts, the high temperature gradient in the pool sets up a strong Marangoni convection. Since, in this time span, the velocity in the molten pool develops quickly, the solution is sensitive to the time step chosen. It is observed that a time step of about 0.002 s lead towards monotonic convergence during this period of initial transience.

Typically, after about 1.5 s, the molten pool reaches a nearly quasi-steady state, when changes in dependent variables between the consecutive time steps are very small. At this stage, slightly higher time steps (typically about 0.005 s) can safely be used to save computational time. After about 2.0 s, when the pool is sufficiently developed, time steps as high as 0.01 s can be implemented. Finally, the computation is carried out upto 3 s to ensure that quasi-steady state has actually been reached. In this period, the maximum relative variations in the values of dependent variables between two consecutive time steps are found to be less than 10^{-5}.

Convergence criteria

Convergence of the dependent variables is checked by method of relative error. Within a particular time step, all the independent variable $(\overline{U}, \overline{V}, \overline{T}, k, \varepsilon)$ values are checked after each iteration. Convergence is declared if the following condition is satisfied at each grid point:

$$\left| \frac{\phi - \phi_{\text{old}}}{\phi_{\max}} \right| \leq 10^{-4} \tag{24}$$

where ϕ is the value of the general variable at a particular grid point at current iteration level, ϕ_{old} is the value of the general variable at the same grid point at the previous iteration level, $\phi_{\max}$ is the maximum absolute value of the same

over the entire domain. It can be noted that numerical simulation of unsteady two-dimensional equations with k-ε modelling is found to be almost 1.5 times CPU expensive than that without turbulence modelling. Each run with k-ε takes about 12 h of CPU time in a Pentium III desktop computer having 128 MB SD RAM and 700 MHz processing speed.

Results of the case study

The temperature field. The temperature distribution for the case study on GTAW is given in Figure 2. From Figure 2, certain important observations can be made regarding the difference in the results between a turbulent simulation and the corresponding laminar simulation. It can be seen from the figure that the asymmetry in the longitudinal section of the weld-pool is more prominent in the laminar case than that in the corresponding turbulent simulation. The above phenomenon can be attributed to the fact that in case of turbulent flow, the diffusion strength is considerably higher than that of the laminar flow, as discussed earlier. Since diffusion is a non-directional phenomenon, the effects of asymmetry imposed by the scanning effect are partially masked by the

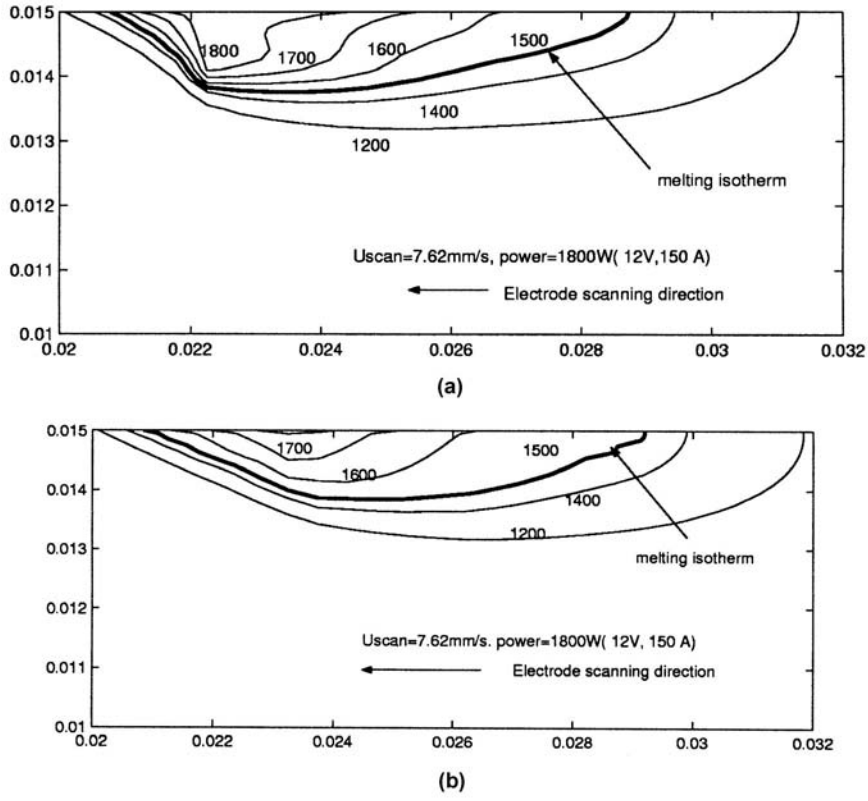

Figure 2.
Temperature contours inside the work-piece corresponding to a current of 150 A, voltage of 12 V, scanning speed of 7.62 mm/s; (a) results of laminar model simulation and (b) results of turbulent simulation. All dimensions are in metres. All temperatures are in °C. The electrode is centred at $x = 0.0225$ m

enhanced diffusion effects, so that the maximum temperature location in case of a turbulent simulation is more towards the centre of the work-piece. Moreover, in the case of laminar simulation, the isotherms are much more crowded towards the direction of scanning near the leading edge of the pool than in the corresponding turbulent case. It can also be noted that the maximum temperature obtained in the laminar case is higher than the maximum mean temperature obtained in the turbulent case, which can be attributed to the high effective thermal diffusivity of turbulent flow, originating from its dispersive nature. It is observed that the high temperature zones have more penetration in laminar simulation than that in the turbulent one.

The velocity field. The velocity vector plot of the laminar simulation and that of the corresponding turbulent simulation for the case study are given in Figure 3. In both cases, the Marangoni flow on the pool surface is radially inward in the direction of maximum surface temperature. The radially inward flow is the result of a positive surface tension coefficient, caused by the presence of surface active elements (such as sulphur and manganese) in steel. From Figure 3, two counter-rotating circulations are observed, both for laminar and turbulent simulations. One small circulation is formed near the melting front of the pool, and another circulation of a larger size covers the rest of the pool. The bigger circulation, which extends up to the trailing edge of the pool, is relatively smaller in size for turbulent flow, as compared to laminar flow. The phenomenon can be explained as follows. In the case of turbulent transport in

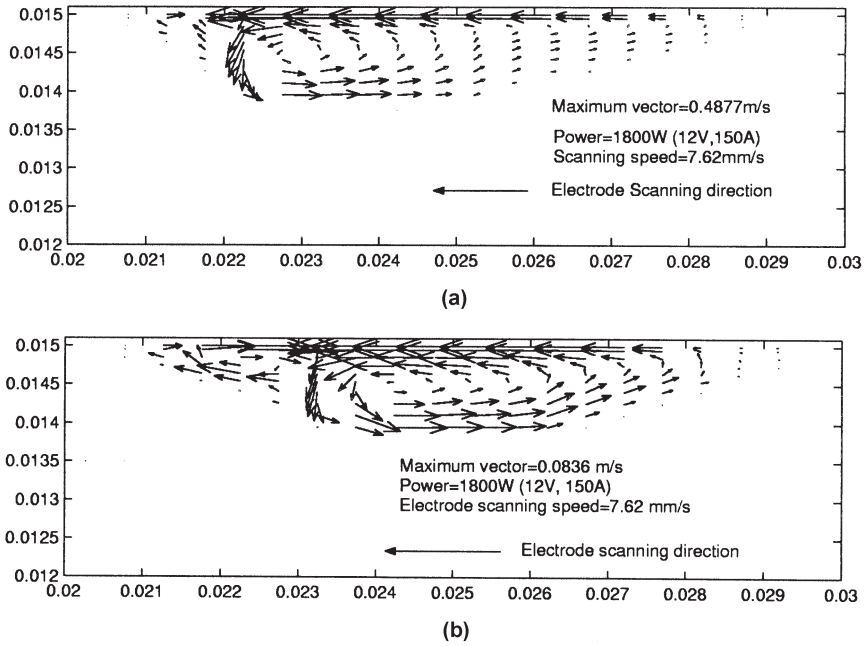

Figure 3.
Velocity vector plots inside the molten pool corresponding to the process parameters as in Figure 2; (a) results of laminar model simulation and (b) results of turbulent simulation. All dimensions are in metres. The electrode is centred at $x = 0.0225$ m

the weld-pool, the maximum mean temperature is much lower than the maximum temperature obtained from the laminar solution, as mentioned earlier. Due to lower temperature gradient in the turbulent pool, the Marangoni convection on the pool surface is weaker than the corresponding laminar case. In this situation, a weak fluid stream coming from the trailing edge of the turbulent pool does not have enough momentum to overcome the flow resistance caused by dynamic pressure of the flow approaching from the melting front. Moreover, the horizontal component of Lorentz force also opposes the flow once it crosses the centre of the work-piece. Hence, the surface flow coming from the trailing edge easily loses its inertia and takes an early turn in the downward direction. This causes the difference in sizes of the vortices for laminar and turbulent situations.

From the earlier explanations, it is also apparent that the effects of Lorentz force on overall pool dynamics appear to be more significant for the turbulent case. To analyse the situation, the distribution of Lorentz force vectors is shown in Figure 4. The force is seen to be symmetrical about the centre of the work-piece. Moreover, for the bigger circulation in the weld-pool, it aids the surface velocity as long as fluid particles are on the right side of middle plane (torch centre). However, once the middle plane is crossed, the horizontal component of Lorentz force vectors tries to oppose the Marangoni flow. Quantitatively, the order of magnitude of the ratio of the electromagnetic force and the inertia force is characterised by the Stuart number (also known as the interaction parameter), given by:

$$\mathrm{N} = \frac{\sigma_{\mathrm{elec}} B_0^2 L}{\rho U} \tag{25}$$

where U and L are characteristic velocity and length scales, respectively, B_0 is the magnetic flux density, and σ_{elec} is the electrical conductivity. For the case presented in this study, we get:

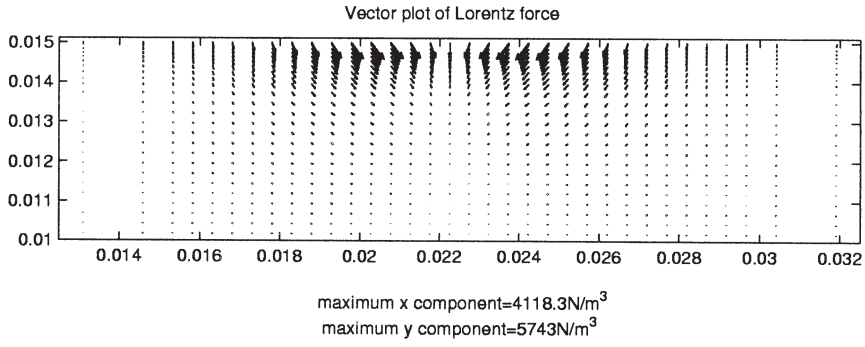

Figure 4.
Vector plot of Lorentz force vector is shown, corresponding to the process parameters as in Figure 2

$$\frac{N_t}{N_l} = 5.8337 \tag{26}$$

where subscripts t and l are used for turbulent and laminar cases, respectively.

From equation (26), it is evident the effect of Lorentz force is of a greater importance in turbulent flow than in the case of a laminar flow.

The weld-pool penetration. The penetration effects in the weld-pool can also be explained in terms of the transport process occurring inside the pool. In case of positive surface tension coefficient (as in the present case), the two fluid streams (one coming from the side of melting front and the other coming from the trailing edge of the weld-pool) turn in the downward direction at the maximum temperature-location on the top surface, thereby carrying thermal energy from the hottest region of the pool to the cooler regions located further down. The downward moving fluid has less momentum in the turbulent pool than in laminar pool. This tends to cause a decrease in turbulent weld-pool depth. On the other hand, the enhanced thermal diffusion tries to increase the penetration of the turbulent pool. These two opposing effects will finally determine the weld-pool depth. The resultant pool depth will depend on several factors such as welding power, surface tension coefficient, scanning speed etc. Hence, it is difficult to conclude, in general, whether a turbulent weld-pool will be deeper than the laminar one, or vice-versa.

Distributions of k, ε and μ_t. The turbulent kinetic energy distribution is shown in Figure 5(a). It can be observed that turbulent kinetic energy becomes a maximum in the vicinity of the top surface of the weld-pool, near the melting front. As the solid from is approached, the magnitude of turbulent kinetic energy decreases. The distribution of dissipation rate of turbulent kinetic energy is shown in Figure 4(b). It can be seen that in the regions where turbulent kinetic energy values are high, the dissipation rates are also high. Also, the maximum rate of dissipation takes place adjacent to the top of the molten pool. Additionally, the location of maximum rate of dissipation is closer to the melting front of the weld-pool. The distribution of μ_t inside the weld-pool is shown in Figure 4(c). It is observed that the value of μ_t decreases as the wall is approached. The highest μ_t is found adjacent to the top surface of the molten pool.

The variation of the earlier turbulent quantities can be explained from Figures 6-9, in which the variations of temperature, velocity, eddy viscosity, turbulent kinetic energy and dissipation rates, with respect to depth as well as along the top surface, are plotted. Figures 6(a) and (b) suggest that the difference between the temperatures predicted by laminar and turbulent simulation is maximum at the top surface of the pool, indicating that the effect of turbulence is there. The dominance of turbulent effect at the free surface is physically meaningful since the top surface is unbounded and the effects of turbulence can manifest themselves in an unrestrained manner at those

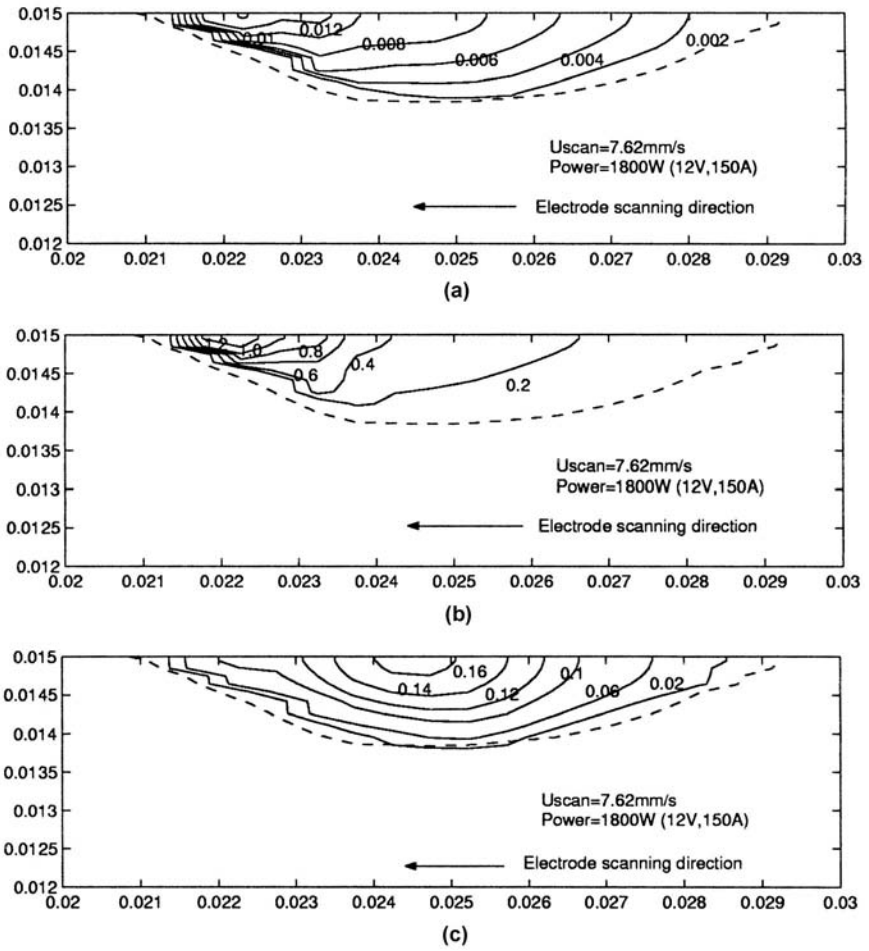

Figure 5.
Distribution of turbulent quantities in the weld-pool, corresponding to process parameter as in Figure 2; (a) turbulent kinetic energy (m^2/s^2), (b) rate of dissipation of turbulent kinetic energy (m^2/s^3) and (c) distribution of turbulent viscosity (Pa s) in the molten pool. All dimensions are in metres. The electrode is centred at $x = 0.0225$ m

locations. This is confirmed from the high values of turbulent kinetic energy at the top surface, which are revealed in Figures 8(a) and 9(a). It can be noted that during the quasi-steady state, in order to maintain local equilibrium, the dissipation rate also should assume a high value, when the turbulent kinetic energy becomes high. Such effects can be seen from Figures 8(b) and 9(b). However, the increase in dissipation rate is not substantial enough to outweigh the effects of enhanced turbulent kinetic energy, which ultimately dictates the net energy exchange between turbulent eddies and the mean flow. Mathematically, the eddy viscosity is a stronger function of turbulent kinetic energy than of the dissipation rate, since it varies with second power of turbulent kinetic energy. Such effects are apparent in Figure 7(b), in which the maximum eddy viscosity at the top surface is attained near the location where

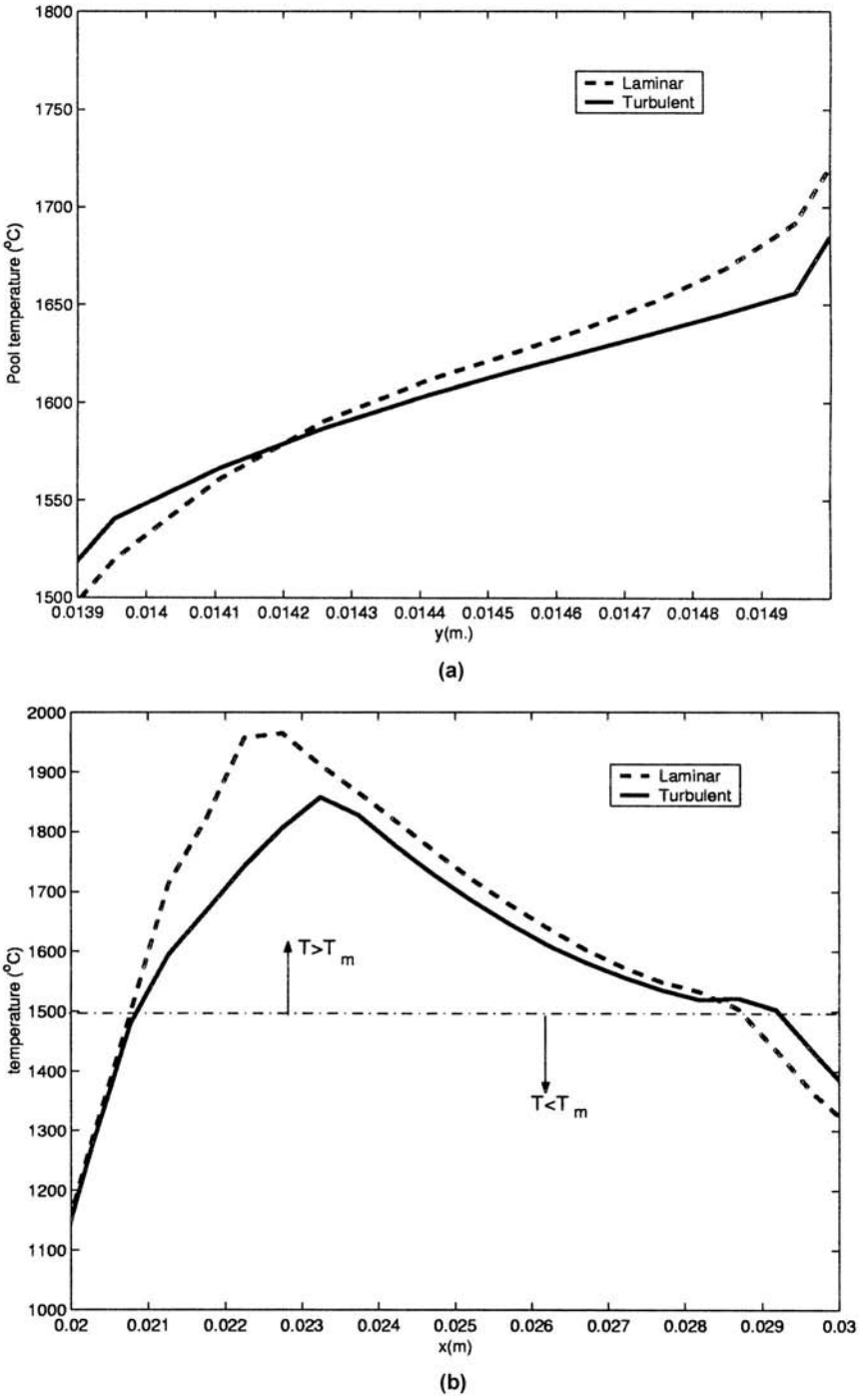

Figure 6.
Comparison of temperature variations between laminar and turbulent models; (a) temperature variation from the bottom to top of the pool at $x = 0.0252$ m and (b) temperature variation at the top surface of the pool along x-direction. The process parameters correspond to those in Figure 2

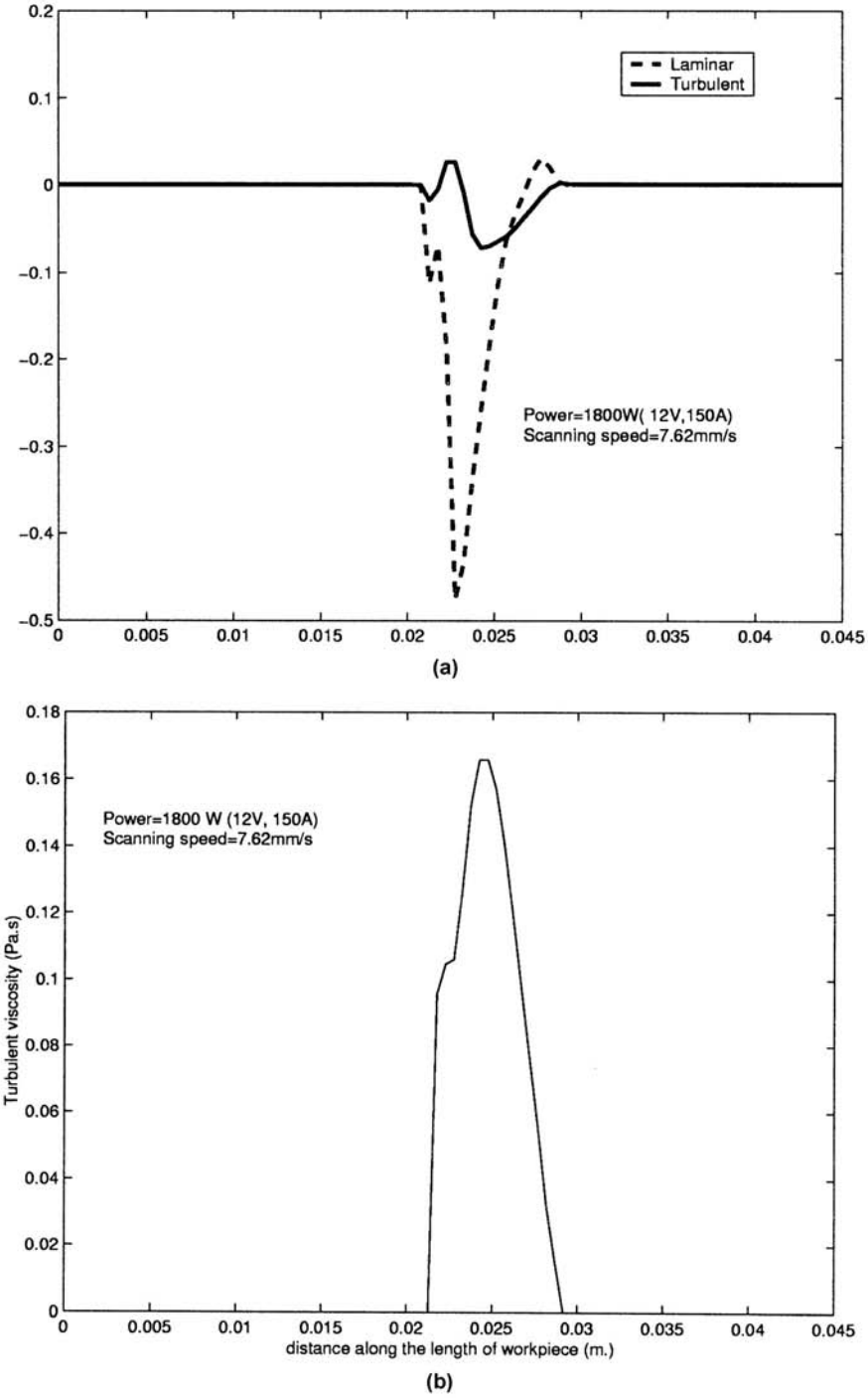

Figure 7.
Variation of flow quantities on the top surface along *x*-direction; (a) variation of top surface velocity along *x*-direction and (b) variation of turbulent viscosity at the top surface along *x*-direction. The process parameters correspond to those in Figure 2

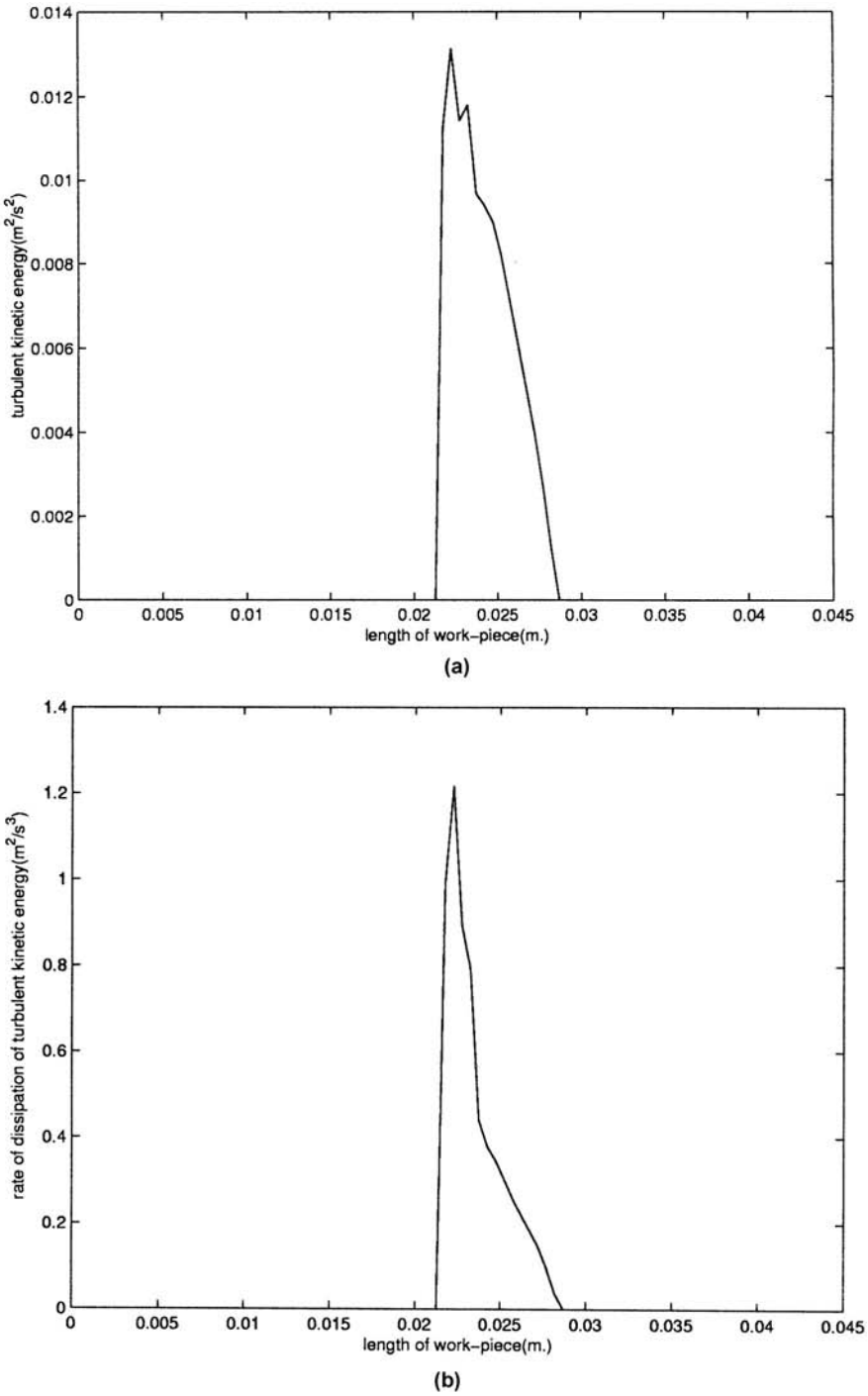

Figure 8.
Variation of turbulent quantities; (a) variation of turbulent kinetic energy at the top surface of the pool along *x*-direction and (b) variation of rate of dissipation of turbulent kinetic energy at the top surface of the pool along *x*-direction. The process parameters correspond to those in Figure 2

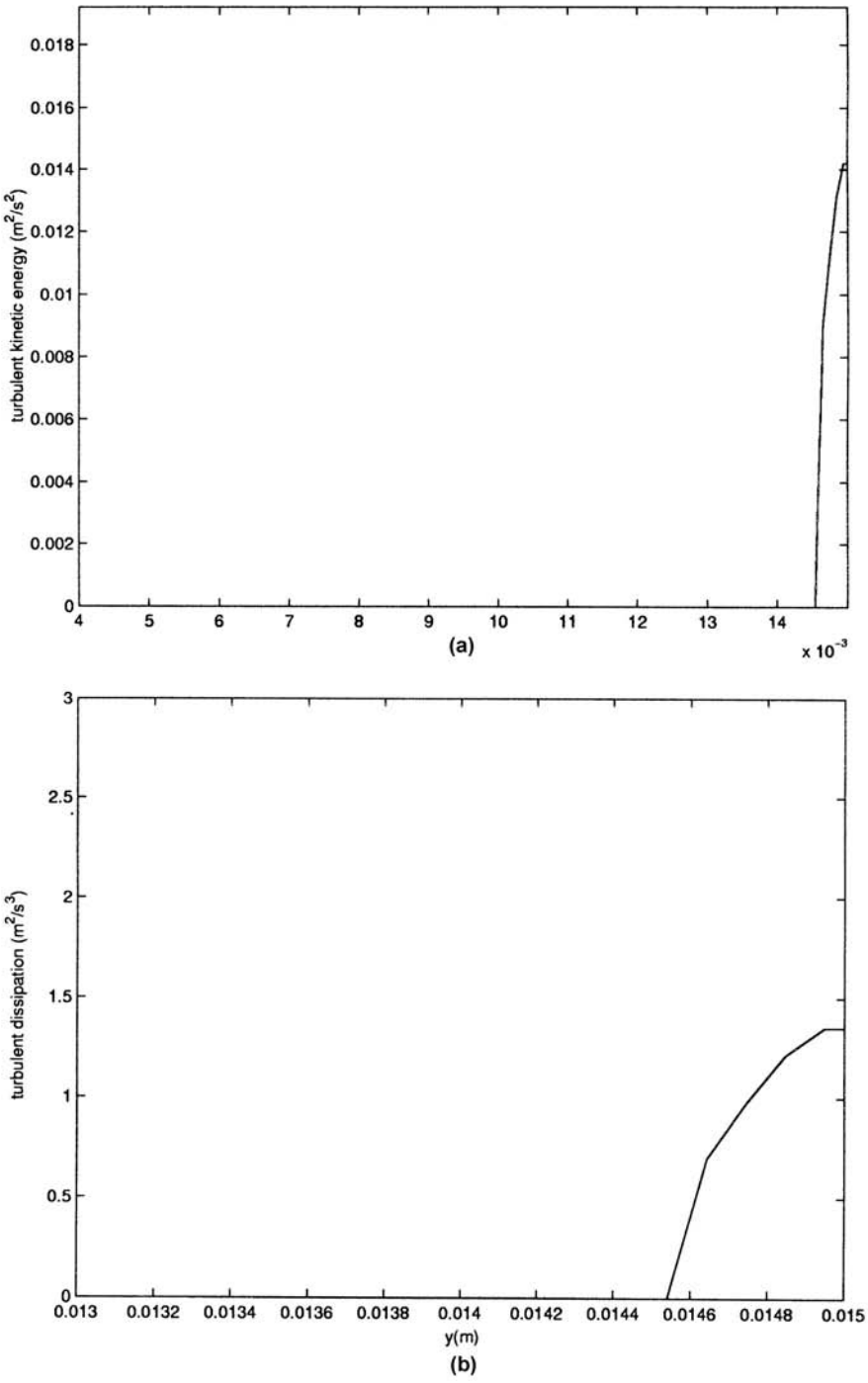

Figure 9.
Variation of turbulence quantities; (a) variation of turbulent kinetic energy from the bottom to top of the pool and (b) variation of rate of dissipation of turbulent kinetic energy from the bottom to top of the pool at $x = 0.0225$ m. The process parameters correspond to those in Figure 2

turbulent kinetic energy attains its maximum value. This high eddy viscosity is responsible for greater degree of diffusion near the top surface of the pool. In fact, the enhanced effects of diffusion during turbulent transport can be easily verified by evaluating the ratio of Peclet number in turbulent transport to that in the laminar transport, which comes out to be about 0.4 in the present case. The earlier ratio indicates that during turbulent transport mechanism in the weld-pool, diffusion is of a greater significance than in the case of laminar transport.

Conclusion

In the present study, a two-dimensional k-ε model is developed for modelling turbulent transport in arc welding applications. From the numerical results, it is evident that turbulent transport phenomena have a marked effect on heat and fluid flow in the weld-pool, resulting in situations strikingly different from the corresponding laminar flow cases. However, the present study is only aimed towards the development of a turbulence model followed by a fundamental investigation revealing some of the important physical issues pertaining to turbulent transport in weld-pools. It is understood that one requires a three-dimensional simulation in order to capture the actual shape of a moving weld-pool. In this regard, we aim to extend the present model to more realistic situations of three-dimensional transport in one of our future investigations.

References

Aboutalebi, M.R., Hassan, M. and Guthrie, R.I.L. (1995), "Numerical study of coupled turbulent flow and solidification for steel slab clusters", *Numer. Heat Transfer*, Vol. 28, pp. 279-99.

Atthey, D.R. (1980), "A mathematical model for fluid flow in a weld pool at high currents", *J. Fluid Mech.*, Vol. 98, pp. 787-801.

Brent, A.D., Voller, V.R. and Reid, K.J. (1988), "Enthalpy-porosity technique for modelling convection-diffusion phase change: application to the melting of a pure metal", *Numer. Heat Transfer*, Vol. 13, pp. 297-318.

Chakraborty, S., Sarkar, S. and Dutta, P. (2001), "A scaling analysis of momentum and heat transport in gas tungsten arc welding", *Science and Technology of Welding and Joining* (in press).

Chang, S.M. (1984), "Prediction of turbulent internal flows with k-ε models", PhD. Dissertation. University of Iowa.

Chao, R.T.C. and Szekely, J. (1994), "The possible role of turbulence in GTA weld pool behaviour", *Weld. J.*, Vol. 73, pp. 25-31.

Correa, S.M. and Sundell, R.E. (1986), "A computational and experimental study of fluid flow in weld-pools", in Kou, S. and Mehrabian, R. (Eds), *Modelling and Control of Casting and Welding processes,* Metallurgical Society, Warrendale, Pennsylvania, pp. 211-27.

Dutta, P., Joshi, Y. and Janaswami, R. (1995), "Thermal modelling of GTAW process with non axisymmetric boundary conditions", *Numer. Heat Transfer, A*, Vol. 27, pp. 499-518.

Hong, K., Wakeman, D.C. and Strong, A.B. (1995), "The predicted influence of turbulence in stationary gas tungsten arc welds", *Trends in Welding Research, Proceedings of 4th International Conference*, Gatinberg, Tennessee, pp. 399-404.

Joshi, Y., Dutta, P., Espinosa, D. and Schupp, P. (1997), "Non-axisymmetric convection in stationary gas tungsten arc weld-pools", *Transactions of the ASME, Journal of Heat Transfer*, Vol. 119, pp. 164-71.

Kanouff, M. and Grief, R. (1992), "The unsteady development of a GTA weld-pool", *Int. J. Heat Mass Transfer*, Vol. 35, pp. 967-79.

Komatsu, T. and Matsunaga, N. (1986), "Defect of k-ε turbulence model and its improvements", *Proceedings of 30th Japan Conference on Hydraulics,* pp. 529-34.

Mundra, K., Debroy, T., Zacharia, T. and David, S. (1992), "Role of thermophysical properties in weld pool modeling", *Weld. J.*, Vol. 71, pp. 313-20.

Oreper, G.M. and Szekely, J. (1984), "Heat and fluid-flow phenomena in weld-pools", *J. Fluid Mech.*, Vol. 147, pp. 53-79.

Patankar, S.V. (1980), *Numerical Heat Transfer and Fluid Flow*, Hemisphere, New York.

Shyy, W., Pang, Y., Hunter, G.B., Wei, D.Y. and Chen, M.H. (1992), "Modeling of turbulent transport and solidification during continuous ingot casting", *Int. J. Heat Mass Transfer*, Vol. 15, pp. 1229-11245.

Further reading

Dutta, P., Joshi, Y. and Frenche, C. (1994), "Determination of gas tungsten arc welding efficiencies", *Exp. Thermal Fluid Sci.*, Vol. 9, pp. 80-9.